AIP | Review of Scientific Instruments

Polymer microfabrication by scanning based microstereolithography: Optical design and material functionality

Ankur Goswami, Arindam Phani, A. M. Umarji, and Giridhar Madras

Citation: Review of Scientific Instruments **83**, 095003 (2012); doi: 10.1063/1.4750975
View online: http://dx.doi.org/10.1063/1.4750975
View Table of Contents: http://scitation.aip.org/content/aip/journal/rsi/83/9?ver=pdfcov
Published by the AIP Publishing

Polymer microfabrication by scanning based microstereolithography: Optical design and material functionality

Ankur Goswami,[1] Arindam Phani,[2] A. M. Umarji,[1] and Giridhar Madras[3,a)]
[1]*Materials Research Centre, Indian Institute of Science, Bangalore 560012, India*
[2]*Instrumentation and Applied Physics, Indian Institute of Science, Bangalore 560012, India*
[3]*Department of Chemical Engineering, Indian Institute of Science, Bangalore 560012, India*

(Received 16 May 2012; accepted 22 August 2012; published online 13 September 2012)

Several research groups have attempted to optimize photopolymerization parameters to increase the throughput of scanning based microstereolithography (MSL) systems through modified beam scanning techniques. Efforts in reducing the curing line width have been implemented through high numerical aperture (NA) optical setups. However, the intensity contour symmetry and the depth of field of focus have led to grossly non-vertical and non-uniform curing profiles. This work tries to review the photopolymerization process in a scanning based MSL system from the aspect of material functionality and optical design. The focus has been to exploit the rich potential of photoreactor scanning system in achieving desired fabrication modalities (minimum curing width, uniform depth profile, and vertical curing profile) even with a reduced NA optical setup and a single movable stage. The present study tries to manipulate to its advantage the effect of optimized lower [c] (photoinitiator (PI) concentration) in reducing the minimum curing width to ~10–20 μm even with a higher spot size (~21.36 μm) through a judiciously chosen "monomer–PI" system. Optimization on grounds of increasing E_{max} (maximum laser exposure energy at surface) by optimizing the scan rate provides enough time for the monomer or resin to get cured across the entire resist thickness (surface to substrate ~10–100 μm), leading to uniform depth profiles along the entire scan lengths. © *2012 American Institute of Physics*. [http://dx.doi.org/10.1063/1.4750975]

I. INTRODUCTION

Over the last decade, advances in microelectromechanical systems (MEMS) have drawn significant attention in the fabrication of complex 3D microstructures for non-silicon based sensor and actuator technologies.[1] Till date, a plethora of techniques has emerged for the fabrication of silicon based MEMS devices.[2] However, extending the same for non-silicon based materials for such technological applications has not been successfully attempted due to limitations on part of silicon based MEMS fabrication techniques. The techniques existing commercially for the fabrication of silicon based MEMS are IC-based micromachining and X-Ray lithographie galvanoformung abformung (LIGA).[3] The former is limited to semiconductor industries only, whereas the latter suffers from high operational cost. The demand for high sensitive non-silicon based MEMS technologies has encouraged the research interests of various groups in developing novel advanced techniques that would make possible the fabrication of non-silicon based complex 3D structures in microdimension. Microstereolithography (MSL) is one such rapid prototyping technique that has emerged over the decade as a feasible technique for microfabrication and is widely being used to fabricate complex 3D non-silicon based structures in microdimensions[4] which finds its utility in fabricating sensors for biomolecular detection, drug delivery, dental applications, and manufacturing of high precision scientific instruments.[5–11]

The technique has evolved considerably from conventional stereolithography[12–15] and it involves the free-form layer by layer microfabrication of a UV sensitive liquid resin by photopolymerization when exposed to UV irradiation.[16] Precisely, a 3D cube can be fabricated through layer by layer stacking of 2D squares, as shown in Fig. 1. The two basic forms of MSL systems, reported widely are based on the mode of radiation exposure, i.e., (A) dynamic mask-based MSL[17,18] and (B) scanning based MSL.[2] The focus of this work has been a scanning based system where a liquid multifunctional monomer in the form of a thin layer of the order of ~10–100 μm over a substrate is selectively exposed to a fixed laser spot focused on to it. The path of the exposed resin is controlled by the movement of the stage automated according to a predefined computer aided design (CAD). Bertsch *et al.* proposed the dynamic mask based MSL system, wherein a 2D thin layer can be fabricated in one shot.[19] Though this system has been adopted by various researchers for its high throughput,[20] it is constrained by pixel resolution and diffraction effects for achieving scaled down dimensions of the order of few microns or sub-microns. The limited depth of field of the order of ~±730 nm of the projected diffraction limited image (for a 0.5 numerical aperture (NA) objective lens and 365 nm working wavelength) in such a system makes it a serious limitation where the desired photoresist layer thickness is typically of the order of ~10–100 microns. Limitations pertaining to minimum achievable feature size were significantly overcome by Levenson by the introduction of phase shifting masks.[21] However, in spite of such modifications, fabrication of large size components by this technique

a)Author to whom correspondence should be addressed. Electronic mail: giridhar@chemeng.iisc.ernet.in.

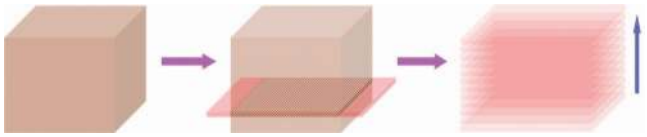

FIG. 1. Layer by layer fabrication protocol in MSL.

demands large size dynamic masks, which inherently limits its flexibility.

On the other hand, scanning based MSL shows much promise where resolution is the primary concern. Five different optomechanical scanning methodologies employed by various groups till date for the development of scanning based MSL are:[2,22–24]

(i) photoreactor scanning (where laser spot is stationary),
(ii) pre-objective galvano mirror scanning,
(iii) post-objective galvano mirror scanning,
(iv) "off-axis" lens scanning, and
(v) scanning systems employing axiomatic design approaches.

However, all the five methodologies are limited with respect to resolution, throughput, and complexity of designs.[25] The first system has the constraint on the speed of scanning in order to prevent the formation of wavy cured patterns thereby limiting the throughput. The wavy patterns are formed mainly due to the unsettling of the low viscous liquid film surfaces for high speed scanning of the motorized stage on which the liquid vat is rested. The second, third, and fourth are inherently limited by the spot characteristics though these methods have high operational throughputs. The fifth system is also limited by the scanning speed and positional accuracy of the focused spot. Gandhi *et al.* suggested a new method of optomechanical scanning designed indigenously where pre-objective galvano scanning is carried out using four mirrors attached to mechatronic arms. This maintains the alignment of the optical axis of the lens with the laser beam in 2D at all times leading to an increase in both resolution and throughput.[25,26] However, their overall mechanical design aspect involves complex custom-designed flexure mechanisms and demands a high level of expertise in mechatronics. The larger number of active movable components in any microfabrication system may lead to errors at each movable stage leading to an overall high error probability in case of precision microfabrication.

Though multiple groups have worked on various aspects of scanning based MSL, discussions on design aspects concerning the material functionalities and beam optics for achieving desired fabrication dimensions with minimal movable parts are not abundant in literature.[4,27–29] The aim of this work has been on the material aspect and optical design in order to exploit the rich potential of photoreactor scanning system for achieving desired scaled down features even with a reduced NA optical setup and a single movable stage. The objective has been on determining the optimization parameters on monomer functionality, choice of initiator, and its concentration. The scan speed of the motorized stage for achieving the desired fabrication modalities (minimum curing width, uniform depth profile, and vertical curing profile) is also optimized. Though this conventional MSL design stands out for its simplicity and higher resolution, it does suffer from a low overall throughput. However, the overall throughput is not a significant factor in microfabrication of specific non-silicon based sensor and actuator structures where the overall fabrication involves the curing of few layers only.

In this paper, we have given a brief overview of the existing literature with discussions on various setups and equations used in MSL. We have focused our efforts on a new setup that uses a reduced NA (as discussed in Sec. II). The common setups that use a larger numerical aperture result in a condensed focus spot and therefore lose on the depth of field of focus (DOF). We have designed and used an optical setup with a higher DOF of the order of ∼1.44 mm without using a conventional beam expander, but at the cost of achieved focus spot diameter. This higher DOF ensures that even if the photoresist or monomer layer thickness is ∼1 mm from the base of the substrate, the spot size will be constant throughout the resist layer. Eventually in our work, we also ensure that the monomer layer thickness is not higher than 300 μm thereby facilitating in obtaining a vertical curing profile. The second aspect of novelty lies in the importance of material functionality, which is extensively discussed in Secs III and IV. MSL literature widely reports the use of higher photoinitiator (PI) concentrations with higher scanning speed and reduced laser exposure energy. However, there is a practical limit to employable scanning speeds for obtaining uniform 3D structures. By judiciously choosing a low PI concentration we are still able to obtain desired curing width dimensions ∼10–15 μm where the working laser focus spot diameter is of the order of ∼21.4 μm. The effect of reducing the PI concentration is twofold: it reduces the curing width and also ensures a uniform vertical curing profile. The third aspect of novelty highlights the optimization of operational parameters with respect to a particular chosen PI concentration in order to obtain uniform curing depth profiles across the scan lengths. Maintaining such a uniform depth profile is imperative for 3D microfabrication.

II. METHODOLOGY OF FABRICATION

A. In house built MSL setup

An in house MSL system has been developed which works on the same vector by vector scanning or raster scanning principle developed by Zhang.[4] The schematic of the setup is shown in Fig. 2(a). It comprises of an argon ion CW tunable laser – Model BeamLok 2065-5S [Spectra Physics, USA], which predominantly radiates at 364 nm monochromatic wavelengths. An acousto-optic modulator (AOM) [NEOS Tech, USA]; optical mirrors [Newport, USA]; 0.5 mm diameter variable aperture [Holmarc, India (inner aperture)]; UV transparent lens with a focal length of 50.2 mm; and *xy-z* coupled linear translational stages (Model -25VP-XL) with XPS-C8 motion controller [Newport, USA] comprise the other essential parts of the MSL system. The laser power is monitored by power/energy meter 842 PE with a detector head 818-P-015-19 [Newport, USA]. The entire setup is mounted on top of a (6′ × 4′) vibration isolation

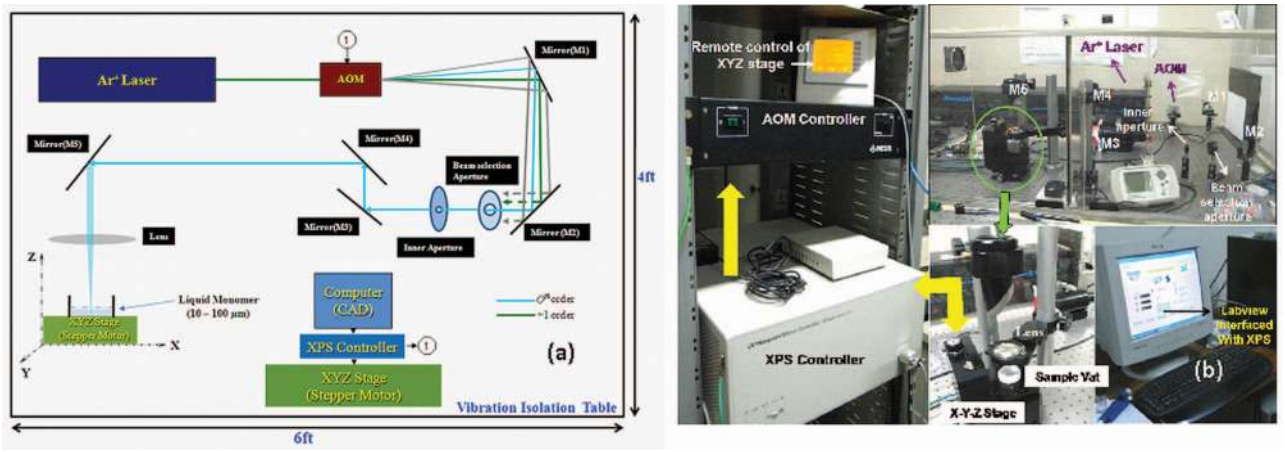

FIG. 2. (a) Schematic diagram of developed MSL setup. (b) Photograph of in-house built MSL system.

optical table RS2000^{TM} [Newport, USA] and is covered by a perspex box in order to achieve dust free environment. The photograph of in house built MSL setup is shown in Fig. 2(b).

Figure 2(a) depicts the beam path through the AOM that falls onto the mirror M1. The AOM diffracts the laser beam into four diffracted orders (−1, 0, 1, 2) when aligned in the beam path along its Bragg angle. Among these, the zeroth order is the continuous beam and splitting of it into diffraction orders is controlled by toggling the input voltage of the AOM between 0 V and 1 V dc. Alignment of the AOM is done so as to concentrate the maximum diffracted power in its first diffracted order (i.e., +1). The variable aperture (inner aperture) is aligned along the first order beam path after passing through another beam selection aperture. This subsequently falls on the mirrors M3, M4, and M5 before it is focused by the converging lens on to the photoresist layer. Thus, by keeping the laser beam path fixed, a thin monomer layer on top of the linear translational stage (automated according to a CAD design interfaced through LABVIEW 8.5.1 [National Instruments]) is subjected to linear predefined scanning based on designed structure (see supplementary material[30]). The design structures are generated through commercial CAD software and exported to the LABVIEW interface after generating standard NC/G-code in order to communicate with the controlling stage and the AOM. The thin monomer layer gets cured line by line following the translational stage movement according to the design. The micrographs of few obtained 2D structures are shown in Secs. IV and V.

B. Laser spot and optical design issues

Obtaining a highly condensed focus spot with a uniform 2D circular irradiance contour (at focus) is imperative for achieving desired minimal feature size with least error in a scanning based optical lithography system. Attempts have been made to improve the throughput by novel scanning schemes of the focused spot, both on-axis and off-axis, though at the cost of spot symmetry for off-axis schemes.[25] In all cases, however, achieving a smaller focus spot is indispensable. Before coming to the point of irradiance contour at focus, it is evident that achieving a higher level of resolution in a scanning based optical lithographic system necessitates the use of a high NA lens for obtaining a desirable minimum achievable focus spot, though at the cost of DOF. For a Gaussian incident beam, the fraction of Rayleigh range Z_R (as shown in Fig. 3) within the photoresist gives an estimate of the $\mathrm{DOF_{working}}$. It is defined as the length along the beam path (photoresist layer to the substrate layer), where the diameter of the beam is no more than $\sqrt{2}$ times its minimum focus diameter and is given by[31]

$$\mathrm{DOF_{working}} = Z_R = \frac{\pi w^2}{4\lambda} \times n_{\mathrm{photoresist}}, \tag{1}$$

assuming that the minimum focus spot is at the bottom of the photoresist layer on the substrate. Here, w is the diameter of the focused spot (measured at $1/e^2$ peak intensity) given by

$$w = \frac{4\lambda f}{\pi d} \times \frac{1}{n_{\mathrm{photoresist}}}, \tag{2a}$$

where diameter of the collimated incident beam (measured at $1/e^2$ peak intensity) is d, working wavelength is λ, effective focal length of the focusing optics is f, and the refractive index of the medium is $n_{\mathrm{photoresist}}$. The NA of the focusing optics is given by

$$\mathrm{NA} = n_{\mathrm{lens}} \sin\theta, \tag{2b}$$

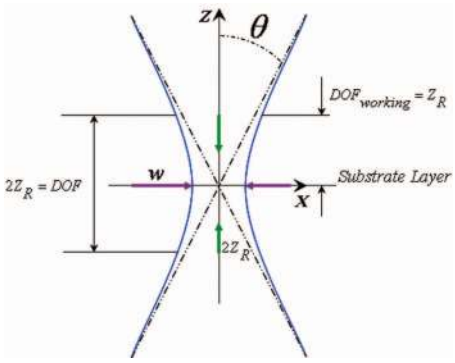

FIG. 3. Schematic of depth of focus of laser beam.

where the half-opening angle of the focused beam is

$$\theta = \tan^{-1}\left(\frac{d}{2f}\right). \quad (2c)$$

Limited DOF of the order of $\sim\pm728$ nm of a diffraction limited spot (for a 0.5 NA objective lens and 364 nm working wavelength) in such a system poses a significant design constraint where the desired photoresist layer thickness is typically $\sim$10–100 μm for each layer of exposure providing for a higher throughput in scanning MSL. Since, DOF gives an estimate of the propagation length, where the beam diameter does not spread significantly from the minimum focus diameter; achieving higher resolution (reduced focus spot) by employing higher NA optics limits the overall working DOF. Such a limitation of shortened DOF in an optical lithographic system nevertheless sets a practical limit on the working NA of the employed optical setup. Practically from the fabrication aspect, the variation of the propagating beam cross section within the photoresist layer leads to significantly undesired non-uniform depth profile of the fabricated structure. This is an issue not widely discussed in MSL literature. The focus of our optical design has been to maintain a $\text{DOF}_{\text{working}}$ of no less than 1 mm, ensuring a reduced error margin in maintaining a uniform beam diameter within the exposed photoresist layer, however, at the cost of a higher focus spot diameter. The overall higher DOF not only allows for a higher photoresist layer thickness ($\sim$300 μm maximum in case of our experiments) per curing layer (improving the overall throughput with fewer curing layers for vertical structures) but also provides a significantly higher degree of freedom ($\sim$even few microns) in maintaining the substrate level under the focusing optics without significant beam divergence with respect to focused diameter within the photoresist layer.

Second, as stated earlier, a condensed focus spot with a uniform 2D circularly symmetric irradiance contour (at focus) is imperative for achieving desired minimal uniform feature size with least dimensional error (both along x and y axes). The effect of intensity contour at focus on the fabricated structure's shape and dimension has not been discussed extensively though it is one of the most essential factors in maintaining the structural modalities for the fabrication of structures of the order of few microns and sub-microns. The variation in the intensity contour (or 2D spot profile at focus) during exposure may distort the desired shape and dimension of the fabricated components. Beam scanning methodologies such as (ii)–(iv) increases the throughput, however, at the cost of intensity profile at focus as discussed in detail by Gandhi and Deshmukh.[26] It is evident that on-axis scanning techniques have a definite advantage over other off-axis scanning schemes in terms of maintaining a uniform spot profile over the entire scanning range. However, limitations of achieving minimal spot size with a rotationally symmetric intensity contour by focusing light waves has been a subject of study over decades.[32–34] It was first theoretically estimated by Richards and Wolf that a linearly polarized Gaussian beam (initially having a rotationally symmetric intensity distribution), when focused by a lens, loses its rotational symmetry at the focus forming an asymmetric deformed focal spot.[33] The perturbation is reflected on the energy density distribution of the longitudinally polarized component at the focus, where the lines of equal intensity at the focus assume the shape of a bone and it is observed to be oriented along the initial direction of linear polarization. For focusing systems with NA $\rightarrow$ 1, the asymmetry is higher though it results in a smaller spot feature at the centre along the cross axis. The theoretical estimations were experimentally verified much later by Leuchs *et al.* while demonstrating sharper focus for a radially polarized annular light beam.[35] Such asymmetric deformations of the intensity contour at focus may significantly distort the desired shape and dimension in a type (i) scanning MSL system.

For linearly polarized beams (as in the case of our laser beam) the area of focal spot, within the limitation of its 2D symmetry, is inversely proportional to the contribution of the rays passing the objective close to the periphery of the objective. This is a condition achievable by a homogenous distribution across the focusing objective. A variable inner aperture (refer Fig. 2(a)) is aligned along the +1 diffracted order beam path and its diameter is adjusted to clip the Gaussian periphery so as to form a homogeneous intensity distribution across the focusing objective. The homogeneous intensity distribution facilitates overcoming the problem of parabolic depth curing profile, as discussed in detail by Schaeffer *et al.*[36] The obtained beam diameter at the focusing optics is measured by a beam profiler [Newport LBP-2-USB] as depicted in Fig. 4 and the measured data is shown in Table I. The focus spot diameter at the working stage (focal length of the objective lens) could not be measured since it is beyond the resolution limit of the profilometer sensor and was estimated to be of the order of $\sim$21.36 μm using Eq. (2a). The $\text{DOF}_{\text{working}}$ with a working NA = 0.0218 (for our design) is estimated using Eq. (1) and is of the order of $\sim$1.44 mm. No beam expander is used in the optical setup in order to maintain the higher $\text{DOF}_{\text{working}}$ and reduce the overall design cost. A beam expander can significantly increase the working NA of the objective lens resulting in even smaller focus diameters but in turn would also increase the intensity side lobes adding to the intensity contour asymmetry,[34] which can pose a serious limitation for precision fabrication. A higher NA setup would have otherwise decreased the $\text{DOF}_{\text{working}}$, which has been a serious consideration in our optical design. The detrimental effect of the higher focused spot size in achieving desired dimensional resolution is overcome by controlling photocuring parameters with respect to material functionalities as discussed in Secs. III and V, which is the main aspect of this work.

TABLE I. Beam profile dimensions at the focusing optics.

	Beam width (Horizontal) (μm)	Beam width (Vertical) (μm)	Mean width (μm)
Min	718.65	648.52	683.58
Max	852.60	768.45	810.53
Aver	777.15	706.01	741.58
STD	28.44	24.86	26.65

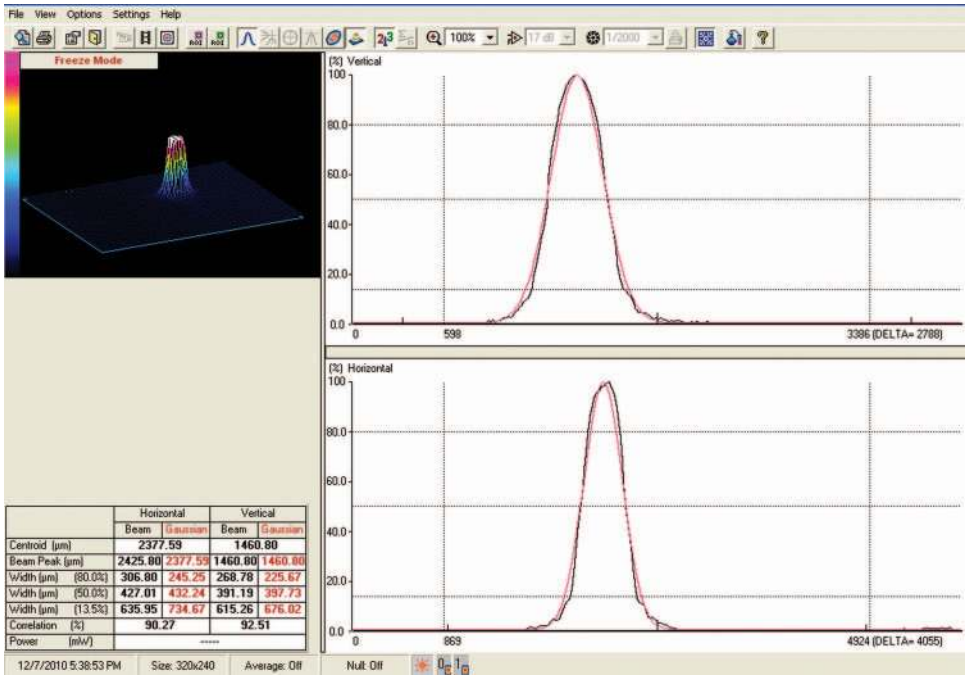

FIG. 4. Laser beam profile and intensity contour of designed setup.

III. PHOTOPOLYMERIZATION PRINCIPLE AND ITS APPLICATION TO MSL

The fundamental aspect of any MSL system involves the photopolymerization of a liquid resin or functional monomer being selectively patterned by UV exposure. Photoinitiated polymerization is brought about by PI which absorb light energy (preferably UV) leading to the formation of free radicals or reactive cations through dissociation. These radicals abstract hydrogen from the resin or functional monomer initiating chain propagation to form polymer as described by the following Scheme 1:[37]

$$PI \xrightarrow{h\nu} R\cdot \xrightarrow{M} RM\cdot$$

$$RM\cdot \xrightarrow{nM} R(M)_n\cdot$$

$$R(M)_n\cdot + R(M)_p\cdot \longrightarrow Polymer$$

SCHEME 1.

Generally in MSL, multifunctional acrylates (with more than one unsaturated double bond) undergo crosslinking in the presence of PI when exposed to UV irradiation, where essentially the polymerization takes place through free radical mechanism. The kinetics of photopolymerization plays an important role in the desired pattern formation and the reaction rate is governed by the initiation efficiency of the photoinitiator, photoinitiator–monomer interaction, the photoinitiator concentration, type of monomer (functionality), and also the viscosity of the monomer. Two types of photoinitiators available commercially are characterized depending on their efficiency and mechanism as Norrish Type I and Type II, where Type I are a more efficient class of photoinitiators compared to the Type II. The Type I photoinitiators undergo photofragmentation in the triplet state forming α cleavages, whereas Type II photoinitiators abstract hydrogen from the monomer to form biradicals upon UV irradiation.[37] Second, monomer functionality greatly influences the photopolymerization kinetics since higher unsaturated double bonds enhance the probability of crosslinking and chain entanglements. The local rate kinetics of free radical photopolymerization R_p varies with the depth of penetration into the resist system and such variation makes it essential to estimate the average polymerization rate for a thickness b of the reaction system.[38] The layered average polymerization rate $\overline{R}_p$ can be derived by integrating the local rate over the layer thickness b and dividing by b, and can be expressed as [39]

$$\overline{R}_p = 2k_p \left(\frac{\Phi I_0 10^3}{2.3\varepsilon\,[c]\,k_t}\right)^{0.5} \left(\frac{1-e^{-2.3\varepsilon[c]b/2}}{b}\right)[M]\,, \qquad (3)$$

where, $k_p$and k_t are the propagation and termination constants of photopolymerization reaction respectively, $[M]$ and $[c]$ are the monomer and PI's initial concentration, I_0 is the incident light intensity at the outer surface of reaction system expressed in units of mol L^{-1} s^{-1}, Φ is the quantum yield of the photoinitiator, ε is the molar extinction coefficient(L mol^{-1} cm^{-1}) and b is the thickness of the exposed monomer layer. Here, k_p, k_t, and ε are the intrinsic properties of the chosen "monomer–PI" system. Increasing the concentration of both PI and incident energy, the local rate kinetics of photopolymerization at the surface can be increased which increases spatial polymerization. In addition, a high quantum yielding (Φ) PI enhances the efficiency of the system to UV absorption. However, higher concentrations of PI have a significant deleterious effect on optical exposure within the "monomer–PI" system as a function of depth resulting in large spatial and temporal variations in local reaction rates. Optical attenuation may be due to higher spatial polymerization rates at

surfaces for higher concentrations of PI which significantly reduces laser penetration depths.[38] Further, higher PI concentrations have the detrimental effect of self quenching.[40] This affects the overall polymerization kinetics across the depth which may result in incomplete conversions across the depth layers from the surface. In order to obtain scaled down microfabricated structures with desired spatial dimensional resolutions and vertical curing profile, it becomes imperative that an optimum layer average reaction rate is essential (high with minimum variation), achievable by lower concentrations $[c]$ of PI, as obvious from Eq. (3). However, a tradeoff lies between rate of polymerization and uniformity of reaction with respect to $[c]$ of PI. For a low concentration, the conversion to polymer would also be small preventing the formation of a gel, which demands optimization of desired fabrication results with regards to uniform depth profile and vertical profile of curing.

The sole dependence of spatial curing dimensions (curing width (C_w) and curing depth (C_d)) on photoinitiator concentration, maximum laser exposure energy at resist surface ($E_{\max}$), scanning speed of the stage (V_s) (along x and y axis), and the penetration depth of the laser beam (D_p) within the resist layer was first reported by the pioneering work of Zissi *et al.*[41] Similar results were reported by Zhang *et al.*[4] The following relations for stereolithography serve as the working equations to optimize the parameters in order to obtain the desired minimum (C_w) and (C_d) in a scanning based MSL system.[42]

The laser exposure energy $E(x/y, z)$ along x or y axis (considering circular symmetry of intensity contour at the focus spot) can be expressed as

$$E\,(x/y, z) = \sqrt{\frac{2}{\pi}}\left(\frac{P}{W_0 V_s}\right)\exp\left(-2\frac{x^2, y^2}{W_0}\right)\exp\left(-\frac{z}{D_p}\right), \tag{4}$$

where W_0 is the radius of the Gaussian beam focus. The maximum exposure energy $E_{\max}$ at the monomer or resist surface is given by $E(0, 0)$ and can be obtained from Eq. (4):

$$E_{\max} = E\,(0, 0) = \sqrt{\frac{2}{\pi}}\left(\frac{P}{W_0 V_s}\right), \tag{5}$$

which is solely a function of operational parameters. The maximum curing depth is also expected to be obtained at the point of x or $y = 0$ where the exposure energy $E(0, z) = E_z$ at the focus spot centre becomes a function of distance z inside the resist layer from the surface and is given by

$$E\,(0, z) = E_z = \sqrt{\frac{2}{\pi}}\left(\frac{P}{W_0 V_s}\right)\exp\left(-\frac{z}{D_p}\right), \tag{6}$$

where D_p represents the maximum penetration depth of the laser beam inside the photoresist layer following Beer-Lambert's law of absorption and is an intrinsic property of the chosen "monomer–PI" system:

$$D_p = \frac{1}{2.303\varepsilon\,[c]}. \tag{7}$$

Experimental results suggest that a typical "monomer–PI" system exhibits a threshold exposure and curing depth following the working curve of Eq. (6) given by[42]

$$C_d = D_p \ln\left(\frac{E_{\max}}{E_c}\right), \tag{8}$$

where the critical exposure E_c represents the minimum energy at the laser wavelength below which curing does not take place. However, Lee *et al.*[43] argued that the empirically derived term E_c is not a constant for a given photochemical system dependant on $[c]$ alone. Instead they derived its dependence as a coupled parameter governed by the intrinsic material properties of the "monomer–PI" system and the processing or operational conditions, where

$$E_c\langle = \rangle \frac{\alpha\beta}{[c]^{1/2}}, \tag{9}$$

α is a factor that involves photochemical parameters, and β incorporates the MSL processing parameters. Intuitively, a smaller value of $[c]$ would increase the critical exposure energy and it is also self explanatory that $E_{\max}$ has to be greater than E_c for at least curing to take place. In effect, smaller the difference ($E_{\max} - E_c$), smaller is the achieved curing depth. This also leads to smaller cured dimensions as well where the curing width as a function of the distance z within the photoresist layer can be reduced to

$$C_w\,(z) = \sqrt{2}W_0\sqrt{\ln\left(\frac{E_z}{E_c}\right)}. \tag{10}$$

Lower $[c]$ also increases the penetration depth D_p and maintains a higher layer average polymerization kinetics (following Eq. (3)) which in turn helps in maintaining a uniform vertical curing profile. This will be elucidated in the discussions of Sec. IV A. Reduction of the polymerization depth by the addition of an unreactive chemical, absorbing highly in the laser wavelength, has also been attempted.[44] However, following the Beer-Lambert's law, such addition of an unreactive photoabsorber is not effective enough in reducing the curing width as it is in reducing the curing depth. Thus, such attempts could not demonstrate the reduction of curing width and depth beyond 40 μm and 150 μm, respectively, even after the use of photoabsorber (tinuvin- P, Sudan I etc), since the amount of photoinitiator considered in fabrication is very high.[41,45]

The significance of material functionality in reducing the curing width and also in maintaining a uniform depth profile by using a lower concentration of PI is discussed further in Secs. IV B and IV C of this paper. Thus, the present work tries to exploit to its advantage the effect of optimized lower $[c]$ in reducing the minimum curing width and also in maintaining a uniform depth profile through a judiciously chosen "monomer–PI" system. Such optimization of the concentration of PI allows the fabrication of microstructures with desired dimensional resolution even with a higher spot size.

A. Material functionalities and MSL operational parameters for microstructure fabrication

1,6 hexane diol diacrylate (HDDA) (80%, Sigma Aldrich, USA) and trimethylol propane triacrylate (TMPTA) (Sigma

Aldrich, USA) are the two multifunctional monomers with different number of unsaturated double bonds chosen.

2,2 dimethoxy 2 phenyl acetophenone (DMPA) (Sigma Aldrich, USA) and benzophenone (BP) (Alfa Aesar) are the Type I and Type II photoinitiators employed for photoinitiation under UV radiation. Both the monomers and DMPA were used as received while BP was twice recrystallized from ethanol. The concentrations of PI $[c]$ in either of the monomers used in this study are maintained in the millimolar (mM) regime so as to manipulate the critical exposure energy E_c, as discussed in Sec. III. The maximum laser exposure energy $E_{\max}$ at the resist surface is varied by changing the stage scan speed keeping the incident laser power constant at 5–6 mW at curing stage (for laser operational stability), ensuring least error in fabrication. The optimizations of the various material functional parameters for achieving desired resolutions of (C_w) and (C_d) have been carried out by fabricating 5×5 mm 2D square mesh structures with subsequent characterizations of (C_w) and scanning depth profile of (C_d) through SEM. The effect of material functionalities on the obtained dimensional resolutions are discussed in detail in Secs. IV A–IV C. Proper characterization through SEM demands the cleaning of uncured monomer after designated laser exposures without the collapse or deformations of the fabricated microstructures due to surface tension effects (stiction effect) at the liquid-solid interface. This is achieved by an indigenously developed process of sublimation drying following the design of Zhang *et al.*,[46] where the excess monomer is first cleansed in a solvent and subsequently solidified at cryogenic temperatures. The frozen solvent is allowed to sublime at a low pressure in a vacuum drying chamber. The details about the sublimation drying apparatus used and the processing technique employed have been discussed in the supplementary information of this paper (see supplementary material[30]). Some of the designed micro-objects and patterns fabricated with all the optimized material functional and operational parameters are shown at the end of the paper.

IV. OPTIMIZATION MOTIVATIONS AND RESULTS

A. Vertical profile control

2D meshes (5×5 mm) were fabricated using the monomers HDDA and TMPTA with different concentrations of BP and DMPA as photoinitiators, where the resist thickness over the substrate is maintained at ~10–100 μm. Figure 5 represents the planar view of one such mesh structure, cured from a solution of 10 mM concentration of BP in HDDA and with a stage scan speed of 0.25 mm/s. The motivation behind the optimization steps has been Eqs. (5)–(10). It is a common observation that C_d depends on the penetration depth D_p of the laser beam within the photoresist layer where the depth depends on the molar extinction coefficient ε of the PI at the wavelength of operation and also the concentration $[c]$ of the PI in the chosen "monomer–PI" system as shown by Eq. (7). Table II shows the molar extinction coefficients of BP and DMPA and their corresponding calculated beam penetration depths D_p in the "monomer–PI" system for the particular concentrations used in this optimization study. Lower values

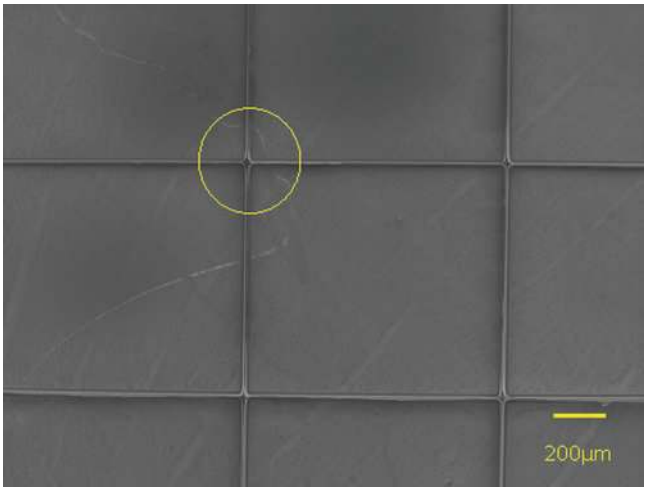

FIG. 5. 2D mesh structure (5×5 mm^2) fabricated from HDDA at 14 mM BP ($\ln E_{\max} = 14.4$ J/m^2) for measuring C_w and depth variation. Circle showing the double exposure at the *x-y* intersection.

of $[c]$ increases D_p and increases the critical exposure energy E_c. Following Eqs. (8)–(10), C_w and C_d solely depend on two distinct parameters:E_c – the material functionality parameter and $E_{\max}$ – the operational parameter. If the difference $(E_{\max} - E_c)$ is smaller, higher is the achievable dimensional resolution.

One of the primary aspects of this work has been in achieving a uniform vertical curing profile with a uniform depth profile along the scan length. Before going into the aspect of depth profile, Eqs. (5) and (6) can be expressed as the following:

$$E_z = E_{\max} \exp\left(-\frac{z}{D_p}\right). \tag{11}$$

The laser exposure energy E_z as a function of the distance z within the photoresist layer derives upon the $(\frac{z}{D_p})$ ratio, the inherent control parameter in maintaining a uniform vertical curing profile. Higher the values of D_p (~few mm), lower will be the decay rate of laser exposure energy E_z at any layer z below the surface of the resist. This ensures $E_z \cong E_{\max}$ where z is of the order of ~10–100 μm. The curing dimensions at any vertical cross section in the resist layer are a function of the laser exposure energy at that cross section. Thus, maintaining a vertical profile of curing becomes a function of the material functionality with regards to PI concentration $[c]$ where the effect of $[c]$ is twofold. Lower values of $[c]$ make $E_c \cong E_{\max}$ and also $E_z \cong E_{\max}$ ensuring uniform laser exposure energy within the resist layer as a function of z thus resulting in uniform vertical profiles. The maximum decay in laser exposure energy with respect to $E_{\max}$ within the photoresist layer is expected to be at the substrate surface where $E_z \Rightarrow E_{\text{substrate}}$. The resist layer thicknesses used in our study (~10–100 μm) were restricted to values much lesser than the calculated D_ps', as represented in Table II. The maximum resist layer thicknesses allowed for validating the claim of uniform vertical profile were of the order of ~300 μm. The calculated values of $E_{\text{substrate}}$ for an 8 mM solution of BP in HDDA and TMPTA are 0.91 $E_{\max}$ and 0.97 $E_{\max}$,

TABLE II. Experimentally determined (UV-Vis spectra) molar extinction coefficient (ε) and calculated penetration depth (D_p).

			Different concentration of PI (mM) [3rd and 5th row] Penetration depth (D_p) (mm) [4th and 6th row]					
	Molar extinction coefficient (ε) (l mol^{-1} cm^{-1})		HDDA					TMPTA
Photoinitiator (PI)	HDDA	TMPTA	8	14	18	25	...	8
Benzophenone (BP)	174	44.5	3.2	1.8	1.4	1.0	...	12.1
2,2 Dimethoxy 2 phenyl	310.9	32.6	1	3	4	6	8	...
acetophenone (DMPA)			14.0	4.7	3.5	2.3	1.75	...

respectively, and that for an 8 mM solution of DMPA in HDDA is 0.84 E_{max}. The higher ($E_{max} - E_{substrate}$) in case of 8 mM solution of DMPA in HDDA prompted optimization steps with lower concentrations in order to maintain vertical curing profiles. For the desired resist layer thicknesses of the order of ~10–100 μm in a photolithographic technique, $E_{substrate}$ for an 8 mM solution of BP in HDDA reduces to an order of ~0.99 E_{max} and 0.97 E_{max} for resist thicknesses of 10 μm and 100 μm, respectively. Even lower resist thicknesses would necessarily mean still smaller differences in laser exposure energy values with respect to E_{max} which in turn would result in finer vertical profiles. Figures 6(a) and 6(b) show the uniform cross-sectional profiles of 2D mesh structures fabricated from 8 mM solution of BP in HDDA ($\ln E_{max} = 15.8$ J/m^2) and TMPTA ($\ln E_{max} = 15.4$ J/m^2) at nearly similar exposure energies. The vertical uniformity profile in case of TMPTA is better compared to that of HDDA owing to the higher value of D_p. Thus, the overall vertical profile uniformity relies on the judiciously chosen "monomer–PI" system and the [c] of the PI which controls D_p along with both E_c and E_z.

B. Uniform curing depth profile across the scan length

After the optimization of the material functionality for maintaining uniform vertical profile has been ascertained on the PI concentration [c] and monomer functionality, we concentrate on the second most important aspect of this study, i.e., maintaining a uniform depth profile along the scan length. In order to obtain desired fabrication resolutions, the concentration of PI has to be optimized so that $E_c \cong E_{max}$. In fact, [c] is optimized in order to increase the critical laser exposure energy values making it comparable to E_{max}. Nevertheless, E_{max} is not an independent parameter and for a scanning based MSL system, it turns out to be an operational parameter dependent on the spot size, the power of the focused beam, and the scanning speed of operation, based on Eq. (5). The spot size and laser power were kept constant at 5–6 mW at the curing stage throughout the study (for laser operational stability). Following Eq. (8), varying the scanning speed would definitely change E_{max} significantly and thereby its effect would also reflect on the curing depth profile of the fabricated mesh structures along the scan length. From the fabrication strategy of meshes (see supplementary material[30]), it is discernable that at the intersection of the two lines, cured twice due to the double exposure (once along x-scan and again along y-scan), a sheer possibility of variation of depth profile can be expected with respect to the curing depth along the rest of the scan lengths of single exposures. Such variations in depth profile are indeed observed for higher scan rates as shown in Fig. 7(a). It is evident that higher scan speeds result in lower exposure energy leading to effective lower curing depths or even incomplete curing for exposure times. These times are not significantly higher than those required for reaching the gel-point for the particular "monomer–PI" system.[12,36,41] Experimental studies of Hirose, Cook, and Standish[47–49] also quantitatively assessed the effects of photoinitiator concentration and light intensity on overall rates, depth of cure, and

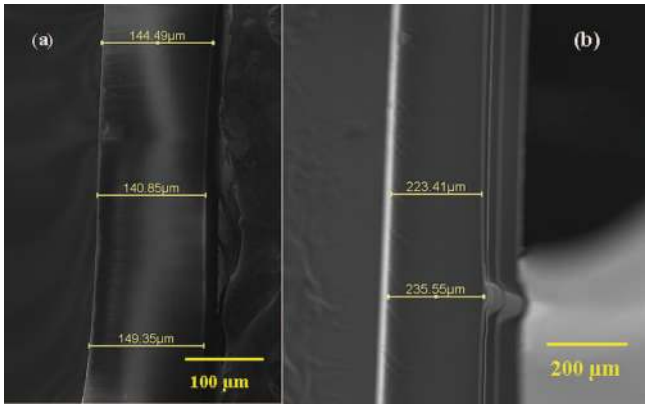

FIG. 6. Cross-sectional view of a mesh structure using BP as a PI at 8 mM concentration from (a) HDDA ($\ln E_{max} = 15.8$ J/m^2) and (b)TMPTA ($\ln E_{max} = 15.4$ J/m^2).

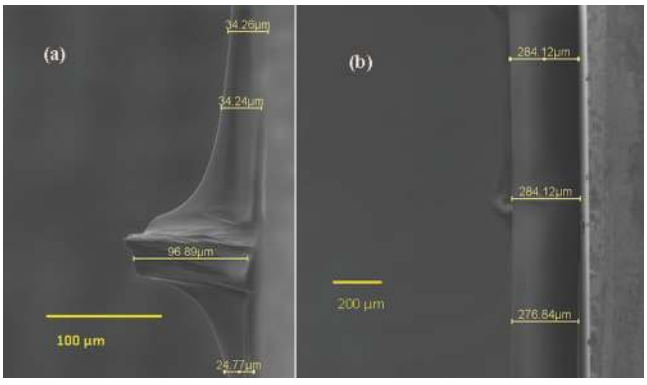

FIG. 7. SEM of depth profile (C_d) of HDDA at 10 mM BP concentration at (a) ($\ln E_{max} = 14.21$ J/m^2) and (b) ($\ln E_{max} = 15.8$ J/m^2).

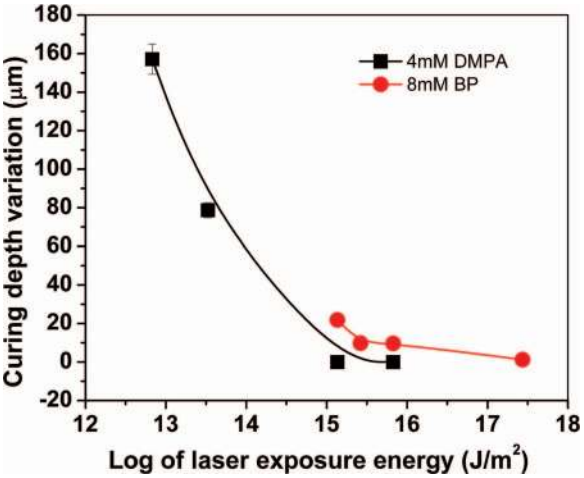

FIG. 8. Variation of depth profile of HDDA mesh structure at different laser exposure energies for BP and DMPA.

final conversion of monomer. Optimization on grounds of increasing E_{max} by optimizing the scan rate and reducing the PI concentration [c] following Eq. (5) nullifies these variations as it provides enough time for the monomer or resin to get cured across the entire resist thickness (surface to substrate). This leads to uniform depth profiles along the entire scan lengths as shown in Fig. 7(b). The variations in depth profile as a function of E_{max} for particular concentrations of BP and DMPA in HDDA are also shown in Fig. 8.

C. Curing width variations

Lowering of scan rates for achieving uniform depth profile across the scan length has a coupling effect on the minimum achievable curing width dimension. For a particular "monomer–PI" system at a higher scan rate, the achieved resolution of curing width is better though at the cost of a non-uniform depth profile along the scan length. As the laser exposure energy is inversely proportional to the scanning speed of the stage, increasing the scanning speed reduces the time of exposure leading to a reduction in curing width and incomplete curing.[36] Thus, optimization of higher E_{max} (for achieving uniform depth profile) sets a fundamental limit to achievable dimensional resolution for a particular "monomer–PI" system. Variations in C_w of HDDA in presence of a fixed concentration of either of BP and DMPA for different scanning rates have been analyzed. Figures 9(a) and 9(b) show the SEM images of a single line of the cured mesh structures of HDDA at fixed laser exposure energy for different concentrations of BP and DMPA. The variations of C_w for different concentrations of PI and varying laser exposure energy have also been carried out. Figures 10(a) and 10(b) show the variations of curing widths as a function of varying laser exposure

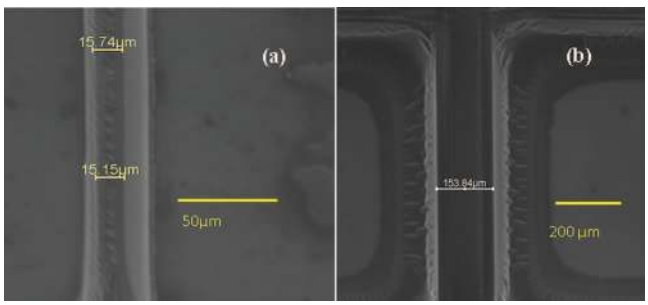

FIG. 9. SEM image of a line of mesh cured from HDDA at ($\ln E_{max}$ = 15.1 J/m^2) laser exposure energy. (a) BP concentration 14 mM and (b) DMPA concentration 6 mM.

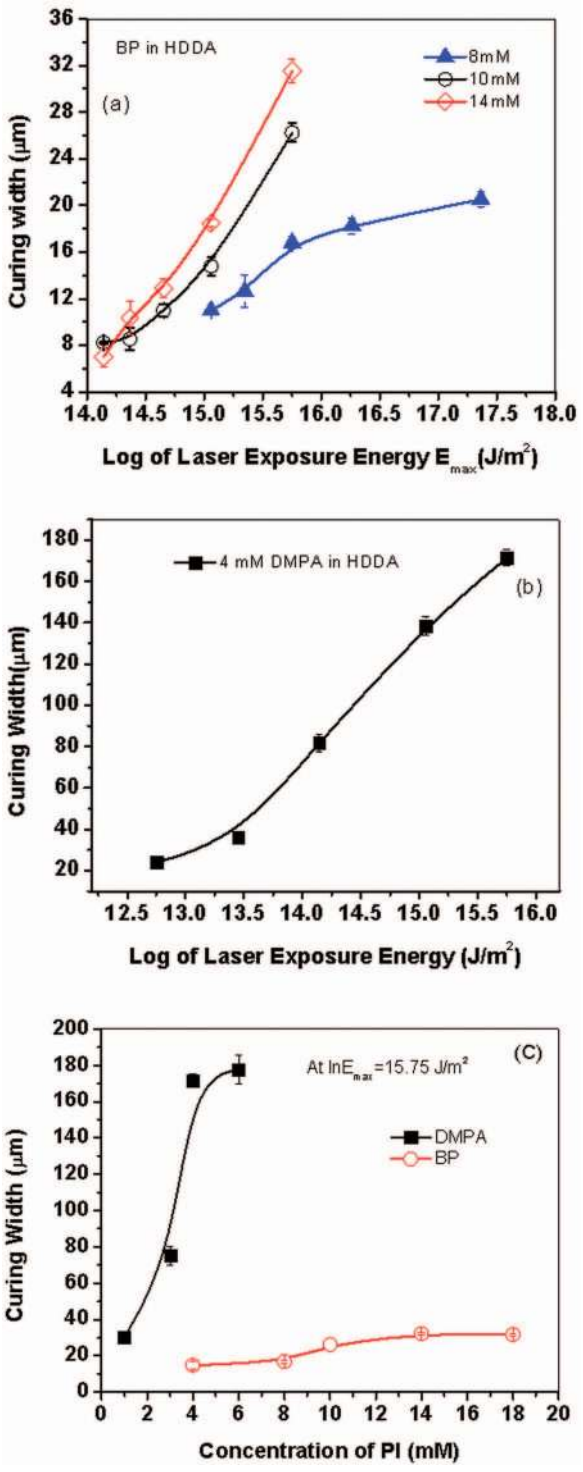

FIG. 10. Variation of curing width (C_w) of HDDA (a) with laser exposure energy at different concentration of BP, (b) at fixed concentration of DMPA, and (c) at different concentrations of PI (BP & DMPA) at fixed laser exposure energy.

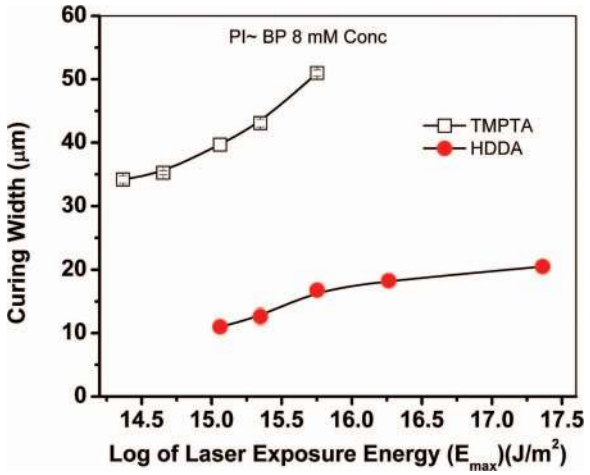

FIG. 11. Variation of curing width (C_w) of TMPTA and HDDA at 8 mM concentration of BP with respect to the laser exposure energy.

energy in presence of BP and DMPA at different concentrations. It is observed that BP exhibits lower curing widths compared to that of DMPA that can be attributed to the higher efficiency of the Norrish Type I (DMPA) with respect to Type II (BP) PI.

The variations of curing width have also been plotted as a function of concentrations of PI for fixed scan speed or exposure energy as shown in Fig. 10(c). The observations are obvious and significantly different for BP and DMPA. DMPA is a more efficient photoinitiator than BP from the aspect of quantum yield. Thus, DMPA has a faster reaction rate than the BP thereby resulting in higher propagation of curing even at lower concentrations. From the fabrication aspect, choice of PI and its concentration should depend upon the desired minimum achievable dimensions.

BP is chosen as the PI to fabricate similar mesh structures with TMPTA and for a comparative evaluation based on monomer functionality. The concentration chosen is 8 mM at which HDDA exhibits minimum curing width and uniform depth profile. Structures were fabricated at this specific concentration with varying scan rates. Figure 11 shows the variation of C_w of TMPTA as a function of exposure energy. Figure 11 also reveals the comparative variation of C_w of HDDA and TMPTA for the same concentration of PI (BP). The observations can be expected because TMPTA contains trifunctional acrylate groups, it exhibits higher reactivity (110 s^{-1}) than HDDA (25 s^{-1}) under UV irradiation.[50] The quenching of PI, which significantly reduces the activity of the PI, depends on the viscosity of the solvent and the quenching constant is given by[37]

$$k_q = \frac{8RT}{3000\eta}, \tag{12}$$

where R is the universal gas constant, T is the temperature in Kelvin, and η is the viscosity in poise. In our studies, laser induced bulk polymerization has been carried out with no added solvent and thus quenching is primarily dominated by the monomer viscosity. TMPTA is a highly viscous monomer (100 mPa-s at 25 °C) compared to HDDA (9 mPa-s at 25 °C) and thus exhibits lesser quenching of PI.[51] Consequently,

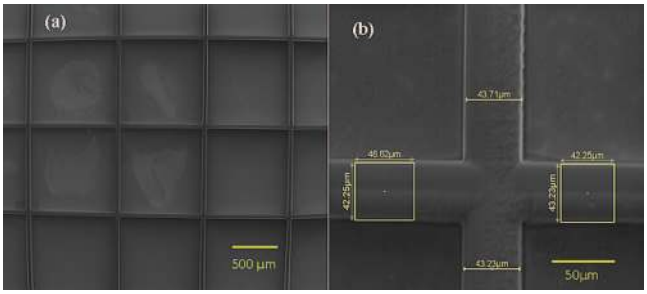

FIG. 12. SEM image of a (a) mesh structure fabricated from TMPTA at 8 mM BP at 15.3 J/m^2 laser exposure, (b) same structure at higher magnification showing uniform C_w and vertical profile.

TMPTA shows three times higher curing widths than that of HDDA for the same concentration of BP at even lower exposure energy.

Figure 12(a) shows a fabricated mesh structure of TMPTA at 8 mM concentration of BP for laser exposure energy of ($\ln E_{\max}$)15.3 J/ m^2. Figure 12(b) depicts the curing width at one cross section of the same mesh cured from TMPTA at same concentration of PI and laser exposure energy. Though the curing width is much higher than that of HDDA at similar concentration and exposure, it shows a more uniform vertical profile. This is expected from the optimization protocol with regards to [c] of photoinitiator as discussed before.

We are able to achieve a minimum curing width of ~7 μm and a minimum curing depth of ~20 μm for HDDA-BP system. Figure 10(a) shows the plot of curing width at different laser exposure energies while Fig. 8 shows the variation of the curing depth with varying concentrations of BP in HDDA.

V. FABRICATION OF FEW 2D AND 3D MICROSTRUCTURES

Some 2D and 3D microstructures have been fabricated using the above optimization parameters. Figures 13(a) and 13(b), respectively, shows the 2D microstructures fabricated from HDDA and TMPTA monomers with 8 mM BP concentration at 15.3 J/m^2 (= $\ln E_{\max}$). Figure 13(a) shows a crosshatch structure whereas Fig. 13(b) depicts the acronym of the authors' institute.

Figures 14(a) and 14(b) show 3D microstructures fabricated using TMPTA with similar PI (BP) concentration and

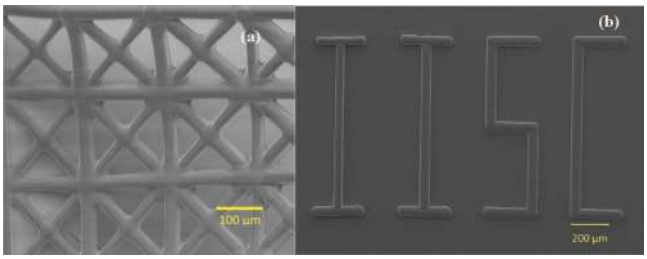

FIG. 13. SEM image of (a) 2D cross hatched structure fabricated from HDDA, (b) fabricated institute acronym at 15.3 J/m^2 laser exposure energy and 8 mM BP concentration.

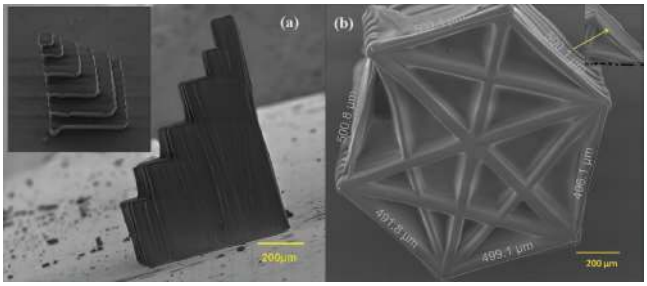

FIG. 14. SEM image of (a) microstairs and (b) cross hatch 3D-hexagonal structure cured from TMPTA monomer at 8 mM BP concentration at 15.3 J/m^2 laser exposure energy.

laser exposure energy. Figure 14(a) depicts microstairs fabricated by stacking of six 2D square layers of consecutive reduced area where the height of each step is 100 μm. Inset shows the stacking of squares to build the microstairs. Figure 14(b) represents a cross hatch 3D-hexagonal structure fabricated by similar stacking of 2D cross hatch hexagons where each side of the hexagon measures 500 μm. The dimension of each side of the fabricated hexagons matches almost with the input dimensions which prove the accuracy of the setup. The inset figure shows the stacking of individual hexagon layers.

Figure 15(a) depicts the top view of an overhanging microcantilever (MC) whose length and width are 500 μm and 200 μm, respectively. Figure 15(b) shows the isometric view of the same microcantilever with a magnified resolution. The MC is fabricated overhanging at a height of 100 μm from the base. Initially, a 3D block of 1 $\times$ 1 $\times$ 1 mm^3 is fabricated with TMPTA-BP (8 mM) solution at exposure energy of 15.3 J/m^2. Similar exposure energy is also used to fabricate the MC structure at one side of the block by maintaining the required monomer layer thickness from the base. The laser penetration depth from the photoresist surface is also optimized through adjustment of the curing stage height. It shows a uniform curing depth across the scan length (as designed $\sim$200 μm following the optimization results as shown in Fig. 6) at a single exposure. The scan length corresponds to the microcantilever length, which is of the order of 500 μm. These two figures (Figs. 14 and 15) prove that the developed system is capable of fabricating 3D micro-objects.

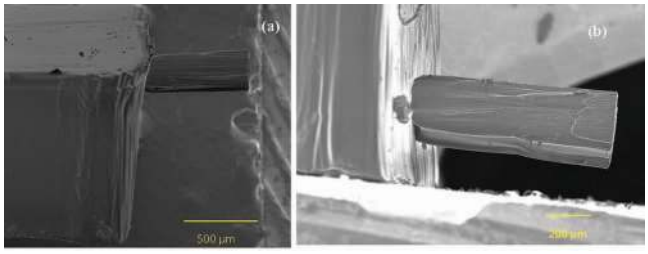

FIG. 15. SEM image of overhang microcantilever structure from a base block at (a) low magnification and (b) high magnification cured from TMPTA monomer at 8 mM BP concentration at 15.3 J/m^2 laser exposure energy.

VI. CONCLUSIONS

Maintaining a uniform depth profile across scan lengths along with a vertical curing profile is one of the main aspects of any scanning based MSL system. It has been a general effort on part of various research groups in fabricating structures primarily with a high PI concentration at the cost of low curing depth and high spatial curing width. The curing line width has been reduced by NA optical setups. This produces a high condensed focus spot but with a loss of intensity contour symmetry and depth of field of focus, which leads to grossly non-vertical curing profiles. Further, such a setup increases the overall cost of the system. This work attempts to revisit photopolymerization process from the aspect of material functionality and optical design in order to overcome these limitations.

In this work, the effects of material functionality along with optimized operational parameters on the fabricated structural modalities have been examined. Material functionality considers reduced photoinitiator concentration and "monomer–PI" system functionality, while the operational parameter optimization involves laser power, laser spot intensity contour, and scanning rate. Contrary to previous efforts, fabricating structures with desired dimensional resolution (even $\sim$10–20 μm curing width) have been demonstrated even with a higher focus spot diameter. This study also allowed us to achieve uniform depth profiles along the scan lengths with vertical profile of curing, providing us with optimized parameters and vital clues for the free form fabrication of 3D microstructures.

Achieving even tighter focus spots with circular symmetric intensity contour by employing radially polarized annular beams, as demonstrated by Leuchs *et al.*,[34,35] can bring down fabricated dimensional resolutions in a scanning based MSL system beyond conventional diffraction limits. Optimizations on grounds of material functionality with regards to polymerization rate kinetics and PI sensitivity can also increase the overall throughput of such a designed system. Present efforts are being concentrated on design and fabrication of polymer based sensor devices for applications in microcantilever sensor technology and also in microfabrication of polymer derived ceramics.

ACKNOWLEDGMENTS

The authors would like to thank the Centre of Excellence in Nanoelectronics (CEN) program, Indian Institute of Science for financial support. Discussions with Professor R. M. Vasu, Department of Instrumentation and Applied Physics, Indian Institute of Science, regarding optical design issues have been very illuminating. The authors would like to express their gratitude to Mr. N. Balashanmugam, Mr. Ankit Krisna, Mrs. L. Sudha and Mr. R. S. Suresh from CMTI, Bangalore for their help rendered in interfacing the *xy-z* stage of MSL system and also in extending their support at various stages of work. The authors are also grateful to IISc AFFM facility for SEM analysis. Mr. Sunil Kumar, from the Physics Department, IISc is also gratefully acknowledged for allowing the use of their laser. The authors thank the anonymous reviewer for constructive suggestions.

[1]P. Dario, M. C. Carroua, N. Croce, M. C. Montesi, and M. Cocco, J. Micromech. Microeng. **5**, 64–71 (1995).
[2]V. K. Varadan, X. Jiang, and V. V. Varadan, *Microstereolithography and Other Fabrication Techniques for 3D MEMS* (Wiley, 2001).
[3]H.-W. Kang, Y.-J. Seol, and D.-W. Cho, J. Micromech. Microeng. **19**, 015011 (2009).
[4]X. Zhang, X. N. Jiang, and C. Sun, Sens. Actuators, A **77**, 149–156 (1999).
[5]A. Goswami, A. Phani, A. Krishna, N. Balashamugam, G. Madras, and A. M. Umarji, in *SPIE Photonics West*, edited by M. A. Maher, J.-C. Chiao, and P. J. Resnick (SPIE, San Francisco, 2011), Vol. 7926, pp. 7926C7921–7910.
[6]J. W. Choi, I. B. Park, Y. M. Hal, M. G. Jung, S. D. Lee, and S. H. Lee, in *SICE-ICASE International Joint Conference* (Bexco, Busan, Korea, 2006), pp. 3678–3681.
[7]A. Phani, M.S. thesis, Indian Institute of Science, Bangalore, 2011.
[8]A. El-Siblani, Proc. SPIE **7596**, 75960G (2010).
[9]D. Cheneler, J. Bowen, S. J. Leigh, C. P. Purssell, D. R. Billson, D. A. Hutchins, and M. C. L. Ward, Ultramicroscopy **111**(8), 1214–1223 (2011).
[10]S. J. Leigh, C. P. Purssell, J. Bowen, D. A. Hutchins, J. A. Covington, and D. R. Billson, Sens. Actuators, A **168**(1), 66–71 (2011).
[11]S. Gittard, P. Miller, C. Jin, T. Martin, R. Boehm, B. Chisholm, S. Stafslien, J. Daniels, N. Cilz, N. Monteiro-Riviere, A. Nasir, and R. Narayan, JOM **63**(6), 59–68 (2011).
[12]J.-W. Choi, R. B. Wicker, S.-H. Cho, C.-S. Ha, and S.-H. Lee, Rapid Prototyping J. **15**(1), 59–70 (2009).
[13]A. Ghosh, in *Rapid Prototyping: A Brief Introduction* (East-West, New Delhi, 1997.).
[14]H. C. Kim, J. W. Choi, E. M. Donald, and R. Wicker, Int. J. Adv. Manuf. Technol. **46**, 1161–1170 (2010).
[15]H. Kim, J. W. Choi, and R. Wicker, Rapid Prototyping J. **16**(4), 232–240 (2010).
[16]S. Takahashi, Y. Kajihara, and K. Takamasu, CIRP Ann. **61**, 219–222 (2012).
[17]I.-B. Park, Y.-M. Ha, and S.-H. Lee, Sens. Actuators, A **167**(1), 117–129 (2011).
[18]H. C. Kim, H. R. Yoon, I. H. Lee, and T. J. KO, J. Adv. Mech. Design Syst. Manuf. **6**(1), 44–51 (2012).
[19]A. Bertsch, P. Bernhard, C. Vogt, and P. Renaud, Rapid Prototyping J. **6**(4), 259–266 (2000).
[20]I. B. Park, Y. M. Hai, M. S. Kim, and S. H. Lee, Int. J. Precis. Eng. Manuf. **11**(3), 483–490 (2010).
[21]M. D. Levenson, Phys. Today **46**(7), 28–36 (1993).
[22]A. Bertsch, S. Jiguet, P. Bernhard, and P. Renaud, Mater. Res. Soc. Symp. Proc. **758**, 2–15 (2003).
[23]S. P. Deshmukh, S. Dubey, and P. S. Gandhi, in Proc. SPIE **6109**, 61090C–61096C (2006).
[24]S. J. Lee, H. W. Kang, T. Y. Kang, G. Lim, J. W. Rhie, B. Kim, and D. W. Cho, J. Micromech. Microeng. **17**, 147–153 (2007).
[25]S. Deshmukh and P. S. Gandhi, J. Mater. Process. Technol. **209**, 1275–1285 (2009).
[26]P. S. Gandhi and S. Deshmukh, J. Micromech. Microeng. **20**, 015035 (2010).
[27]J. Choi, Y. M. Ha, S. H. Lee, and K. H. Choi, J. Mech. Sci. Technol. **20**(12), 2094 (2006).
[28]A. Bertsch, S. Jiguet, and P. Renaud, "Microfabrication of ceramic components by microstereolithography," J. Micromech. Microeng. **14**, 197–203 (2004).
[29]J. W. Choi, E. MacDonald, and R. Wicker, Int. J. Adv. Manuf. Technol. **49**, 543–551 (2010).
[30]See supplementary material at http://dx.doi.org/10.1063/1.4750975 for laser curing strategy; and for sublimation drying.
[31]T. E. Schäffer, in *Applied Scanning Probe Methods V*, edited by B. Bhushan, H. Fuchs, and S. Kawata (Springer, 2007), Vol. V.
[32]R. P. Feynman, R. P. Leighton, and M. Sands, *The Feynman Lectures on Physics* (Narosa Publishing House, New Delhi, 2003).
[33]B. Richards and E. Wolf, Proc. R. Soc. London, Ser. A **253**, 358–379 (1959).
[34]S. Quabis, R. Dorn, M. Eberler, O. Glöckl, and G. Leuchs, Opt. Commun. **179**, 1–7 (2000).
[35]R. Dorn, S. Quabis, and G. Leuchs, Phys. Rev. Lett. **91**(23), 233901–233904 (2003).
[36]P. Schaeffer, A. Bertsch, S. Corbel, J. Y. Jezequel, and J. C. Andre, J. Photochem. Photobiol. A **107**, 283–290 (1997).
[37]A. Raave, *Light-Associated Reactions of Synthetic Polymers*, (Springer, New York, 2006).
[38]G. Terrones and A. J. Pearlstein, Macromolecules **34**, 3195–3204 (2001).
[39]G. Odian, *Principles of Polymerization*, 4th ed. (Wiley, New York, 2007).
[40]D. K. Balta, N. Arsu, Y. Yagci, S. Jockusch, and N. J. Turro, Macromolecules **40**, 4138–4141 (2007).
[41]S. Zissi, A. Bertsch, J.-Y. Jezequel, S. Corbel, D. J. Lougnot, and J. C. Andre, Microsyst. Technol. **2**, 97–102 (1996).
[42]P. F. Jacob, *Stereolithography and Other RP&M Technologies* (Society of manufacturing Engineers, Dearborn, 1992).
[43]J. H. Lee, R. K. Prud'homme, and I. A. Aksay, J. Mater. Res. **16**(12), 3536–3544 (2001).
[44]E Manias, J. Chen, N. Fang, and X. Zhang, Appl. Phys. Lett. **79** (11), 1700–1702 (2001).
[45]R. Ibrahim, M. H. H. Ramlee, M. A. S. Mohamed, M. Ibrahim, and M. S. Wahab, Appl. Mech. Mat. Adv. Manuf. Technol. Syst. **159** 109–114 (2012).
[46]D. Wu, N. Fang, C. Sun, and X. Zhang, Sens. Actuators, A **128**(1), 109–115 (2006).
[47]W. D. Cook and P. M. Standish, Aust. Dent. J. **28**(5), 307–311 (1983).
[48]W. D. Cook, J. Appl. Polym. Sci. **42**, 2209–2222 (1991).
[49]T. Hirose, K. Wakasa, and M. Yamaki, J. Mater. Sci. **25**(2), 1209–1213 (1990).
[50]C. Decker, Prog. Polym. Sci. **21**, 593–650 (1996).
[51]K. Studer, C. Decker, E. Beck, and R. Schwalm, Prog. Org. Coat. **48**(1), 92–100 (2003).